

## A Tale of Two Helicopters

Srikanth Saripalli<sup>1</sup>, Jonathan M. Roberts<sup>2</sup>, Peter I. Corke<sup>2</sup>, Gregg Buskey<sup>3,2</sup>

Gaurav S. Sukhatme<sup>1</sup>

<sup>1</sup>Robotics Research Lab, University of Southern California  
Los Angeles, USA

<sup>2</sup>CSIRO Manufacturing & Infrastructure Technology  
PO Box 883, Kenmore, Qld 4069, Australia

<sup>3</sup>University of Queensland  
St. Lucia, Qld 4066, Australia

### Abstract

*This paper discusses similarities and differences in autonomous helicopters developed at USC and CSIRO. The most significant differences are in the accuracy and sample rate of the sensor systems used for control. The USC vehicle, like a number of others, makes use of a sensor suite that costs an order of magnitude more than the vehicle. The CSIRO system, by contrast, utilizes low-cost inertial, magnetic, vision and GPS to achieve the same ends.*

*We describe the architecture of both autonomous helicopters, discuss the design issues and present comparative results.*

### 1 Introduction

Recent joint work between USC and CSIRO has provided a unique opportunity to compare independently developed helicopter control architectures. We discovered some small differences in the control loop structure but the biggest difference by far is the performance and cost of the sensor suites used.

In Table 1 we present, to the best of our knowledge, a summary of each of the currently active autonomous helicopter projects including [1–3]. A common feature of all but the CSIRO system is that they utilize high-performance, avionic grade sensors. These sensors are expensive, typically exceeding the cost of the vehicle by one order of magnitude. These devices, such as the Novotel RT2 Millennium and the Trimble TANS Quadrex, provide good quality information about the state of the vehicle at 10Hz which greatly simplifies the state-estimation and control problem.

The CSIRO project has, from its inception, aimed to develop a control system using low-cost sensors, and initially



Figure 1: The CSIRO helicopter.



Figure 2: The USC helicopter.

not considering GPS at all. Its primary sensors are low-cost inertial, magnetic and stereo vision. The first two run at 76Hz which is sufficient to control the attitude of the helicopter while the latter runs at 5Hz to facilitate veloc-

ity and position control. The stereo vision system provides height relative to the ground (unlike GPS which gives less useful absolute height) and also speed from optical flow between consecutive frames.

Our current joint work provides a good opportunity to explore the design trade-offs and other issues between one example of an “expensive sensor” helicopter, and the “low-cost sensor” helicopter. The sensor suite of the CSIRO helicopter is described in [4]. The USC helicopter is described by Saripalli [5]. This paper deals mainly with the CSIRO helicopter on which members from both project teams worked.

University	Sensors and processing techniques used on the Helicopter
Massachusetts Institute of Technology	<ul style="list-style-type: none"> <li>• X-Cell 60 Helicopter</li> <li>• ISIS-IMU with 100Hz update rate and 0.02 degrees/minute drift</li> <li>• Honeywell HPB200A Altimeter with 2ft accuracy</li> <li>• Superstar GPS receiver from Marconi with 1 Hz update rate</li> <li>• 13-state extended Kalman filter for state estimation</li> <li>• LQR based control</li> </ul>
Carnegie Mellon University	<ul style="list-style-type: none"> <li>• Yamaha R-Max Helicopter</li> <li>• Litton LN-200 IMU with 400 Hz update rate and <math>\leq 1ms</math> latency</li> <li>• Novatel RT-2 differential GPS with 2cm accuracy</li> <li>• KVH-100 flux-gate digital compass with 5 Hz update rate</li> <li>• 12-state extended Kalman filter for state estimation</li> <li>• Control based on <math>H_{inf}</math> control</li> </ul>
Stanford University	<ul style="list-style-type: none"> <li>• X-Cell 60 Helicopter</li> <li>• Trimble TANS Quadrex GPS with 3cm position accuracy</li> <li>• Used GPS with multiple antenna for attitude estimation</li> <li>• No other sensors used</li> <li>• State estimated using custom algorithms from carrier phase GPS</li> <li>• PD based control</li> </ul>
Georgia Institute of Technology	<ul style="list-style-type: none"> <li>• Yamaha R-50 Helicopter</li> <li>• ISIS-IMU with 100Hz update rate and 0.02 degrees/minute drift</li> <li>• Novatel RT-2 differential GPS with 2cm accuracy</li> <li>• Radar and Sonar Altimeters</li> <li>• HMR-200 triaxial magnetometers</li> <li>• 17-state extended Kalman filter for state estimation</li> <li>• Feedback linearization with neural networks for control</li> </ul>
University of California Berkeley	<ul style="list-style-type: none"> <li>• Yamaha R-Max Helicopter</li> <li>• Boeing DQI-NP INS/GPS integration system</li> <li>• Novatel RT-2 differential GPS with 2cm accuracy</li> <li>• DQI-NP unit provides attitude, velocity and position information</li> <li>• No state estimation necessary since the sensors provide state</li> <li>• <math>H_{inf}</math> based control</li> </ul>
University of Southern California	<ul style="list-style-type: none"> <li>• Bergen twin Industrial Helicopter</li> <li>• CrossBow VGX IMU with 133Hz update rate and 2 degrees accuracy</li> <li>• Novatel RT-2 differential GPS with 2cm accuracy</li> <li>• TCM-250 triaxial magnetometer</li> <li>• Laser altimeter with 10 cm accuracy and 10 Hz update rate</li> <li>• 16-state Kalman filter for state estimation</li> <li>• PID based control</li> </ul>
CSIRO	<ul style="list-style-type: none"> <li>• X-Cell 60 Helicopter</li> <li>• Custom made IMU embedded with magnetometers with 76 Hz update rate</li> <li>• Ublox GPS unit with differential corrections using WAAS, 2m accuracy</li> <li>• Stereo vision for height estimation</li> <li>• Velocity estimation using vision</li> <li>• Complimentary filters and extended Kalman filter used in conjunction</li> <li>• PID based control</li> </ul>

Table 1: Sensor suites, state estimation and control approach for some contemporary projects.

The remainder of the paper is organized as follows. Section 2 discusses the state estimation techniques used by the CSIRO helicopter. Section 3 describes the different control approaches used by CSIRO and USC, and includes experimental results. Finally, Section 4 lists some conclusions.

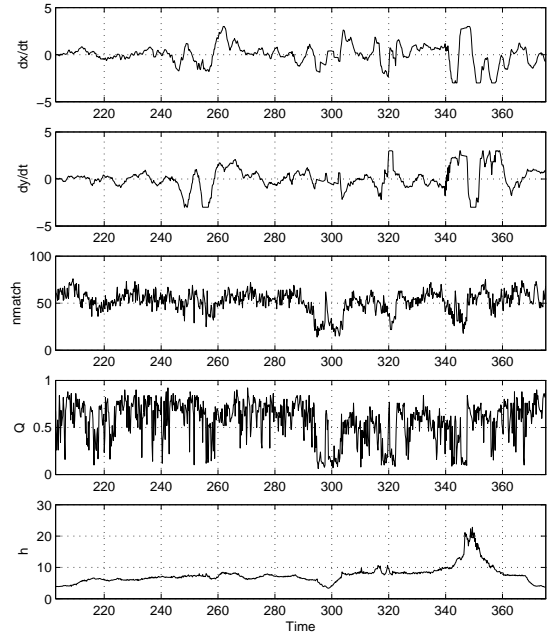


Figure 3: Online vision based velocity and height results.

## 2 State estimation

### 2.1 Vision

WeThe CSIRO team use vision to provide estimates of vehicle height and motion at 5 Hz from images of natural undulating grassy terrain with no artificial landmarks. The estimates of  $h$ ,  $\dot{x}$  and  $\dot{y}$  are all in the body-fixed frame.

Tracking corner features between consecutive frames provides the raw information for velocity estimation and odometry. Since the corners are already computed for the stereo process we do not have to recompute them for motion estimation. The two subproblems are correspondence and motion estimation, which are not independent. Currently we use a simple strategy for establishing correspondence which assumes that the matching points lies within a disk of fixed radius from a point predicted based on attitude change from the previous frame.

For each frame we typically achieve at least 20 strong matches but there are frequently a large number of spurious matches, since there is no apriori epipolar constraint. More details are provided in [4]. A number of robust techniques including ICP and vector median filtering are used to establish a consensus velocity.

The significant issues are computational complexity and robust estimation that can handle mismatched features. The algorithms are implemented as tightly written C code

and executes in around 80ms on the helicopter's 800MHz P3 processor.

Figure 3 shows the results of the vision based velocity and height estimation. The top two plots show the velocity in the x and y directions respectively as computed by the velocity complementary filter. The third and fourth plots show the number of tracked features and the quality measure. This quality measure is the ratio of the number of consensus velocity features divided by the total number of features. Finally, the bottom plot shows the height as computed by the stereo vision algorithm.

## 2.2 Inertial sensors

A custom built low-cost IMU and magnetic compass were developed for the CSIRO helicopter. The combined unit is known as the Embedded inertial Measurement Unit, EiMU, pronounced "emu" like the bird (Figure 4). The EiMU is actually an Attitude and Heading Reference System (AHRS). The inertial sensors are three Murata ENC-03J solid-state rate gyros and two Analog Devices dual-axis ADXL202JQC accelerometers. The unit also contains three Honeywell HMC1001/2 magnetometers.

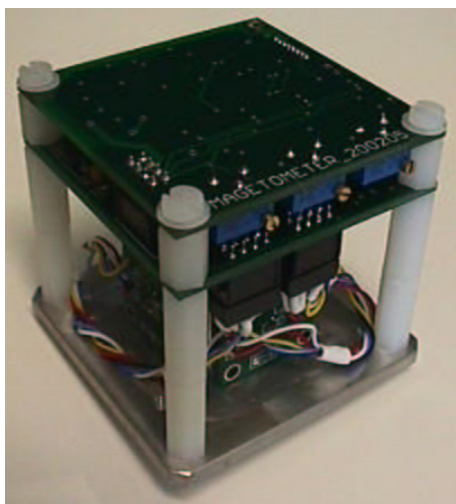


Figure 4: The EiMU.

The accelerometers are well calibrated, but the gyros are not. The gyros have a significant time-varying rate bias. Originally, a complementary filter was used in order to determine the attitude of the helicopter [4]. The complementary filter gave reasonable results and closed-loop attitude control was achieved using it. However, the complementary filter does not deal with the gyro rate bias well and an extended Kalman filter was implemented to address this issue.

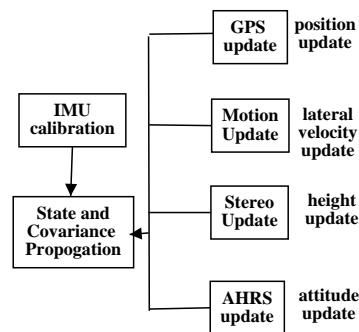


Figure 5: Kalman Filter

## 2.3 Overview of the Extended Kalman Filter

To implement full state feedback control on a helicopter we use an extended Kalman filter to merge the sensor information from the inertial measurement unit (IMU), differential global positioning system (DGPS), and vision-system derived height and velocity estimates. An extended Kalman filter is used to optimally combine each of the on-board sensors given unique update rates, error characteristics and coordinate frames. The core of the filter is provided by the IMU which propagates the helicopter state vector over time. An helicopter dynamic model is not used, instead the measured accelerations and the rotational velocities provide the inputs for the rigid body motion equations. Although this is just an approximation to the more accurate model including the full aerodynamics of the helicopter, this allows us to operate in more flexible situations, such as when the helicopter is in air, or on the ground or even bolted to a car for testing without changing the model of the helicopter. The block diagram in Figure 2.3 shows the relationship between various sensors.

### 2.3.1 System Model

A typical dynamic system model used in Kalman filtering has the following model [6]

$$\frac{d}{dt}X = \dot{X} = f(X, u) + W N(0, Q) \quad (1)$$

Here  $X$  is the system state, ' $f$ ' is the system function and ' $u$ ' represents the forces such as gravity, lift, torques etc acting on the aerodynamic structure and acting it to move. But without a validated full model of the helicopter dynamics, we cannot determine what ' $u$ ' is. Instead we use the accelerations from the IMU and the rotational velocities from the IMU to substitute for the control inputs in driving the motion dynamics. The noise inherent in the measurements is incorporated in the process noise

The measurement noise present in the inertial readings is lumped together with the process noise  $W$  and propagated to the state variable error covariance during the prediction loop.

$$\dot{X} = f(X, \bar{a}\bar{\omega}) + W N(0, Q) \quad (2)$$

where the measured accelerations  $\bar{a} = (\bar{a}_x, \bar{a}_y, \bar{a}_z)$  and the measured rotational velocities  $\bar{\omega} = (\bar{\omega}_x, \bar{\omega}_y, \bar{\omega}_z)$  are parameters of the system function  $f(\cdot)$ .

### 2.3.2 System States

The system states contain the navigational parameters which are tracked and filtered by the extended Kalman filter. The choice of a state vector is largely determined by trade-off between filter complexity and accuracy. In this case the state consists of the position of the helicopter in the local co-ordinate frame of reference, the velocity of the helicopter in the body co-ordinate frame, attitude of the helicopter, the gyroscope biases and the magnitude of the gravity vector. Quaternions are used for representing the attitude instead of Euler angles to take care of the singularities. Gravity is included as a state because it when used in conjunction with roll and pitch allows the DGPS discrete updates to handle larger changes in the bias errors in the inertial accelerometer measurements. By giving the Kalman filter this extra degree of freedom the gravity vector takes up the slack from the accelerometer biases

The 14 states of the navigation filter consist of  $x_L, y_L, z_L$ , the position of the helicopter with respect to a ground reference expressed in the local frame,  $u_B, v_B, w_B$  the helicopter velocities expressed in the body frame,  $e_0, e_1, e_2, e_3$ , the attitude parameters represented as a quaternion, the gyro biases represented by  $p_{bias}, q_{bias}$  and  $r_{bias}$  and the magnitude of the gravity vector  $g$ .

The rotational bias states  $p_{bias}, q_{bias}, r_{bias}$  provide a continuous estimate of the current drift in the gyroscopes of the IMU. These biases are used when converting the raw IMU rotational velocities into measured rotational velocities. For example

$$\bar{\omega} = \omega_{raw} - \omega_{bias}$$

where  $\omega_{raw}, \omega_{bias}, \bar{\omega}$  are respectively the raw, biased and measured rotational velocities in radians/sec. The rotational biases vary dynamically due to parameters such as instrument temperature or acceleration.

### 2.3.3 Kalman Filter Equations

The extended Kalman filter has two phases. In the first phase, the estimate state vector  $\hat{X}(t)$  is propagated by

the underlying continuous-time nonlinear system dynamics and its corresponding error covariance matrix  $P$  is propagated by a linearized state dynamics matrix  $A$ . In the second phase, discrete-time measurements update the state estimate with the optimal Kalman gain matrix  $K$ , and the error covariance matrix is correspondingly adjusted.

## 2.4 Propagation Phase

The propagation of the state vector is based on the rigid body equations of motion and has the following form

$$\dot{\hat{X}}(t) = f(\hat{X}(t), t, \bar{\omega}(t), \bar{a}(t)) \quad (3)$$

where  $\hat{X}$  is the state vector and  $\bar{\omega}$  and  $\bar{a}$  are the inertial measurements, angular rate and acceleration respectively.

The non-linear system function is linearized about the current state estimate to produce the linearized system matrix  $A$  which is the Jacobian of the system states and is given by [7]

$$A(\hat{X}(t), t, \bar{a}\bar{\omega}) = \left. \frac{\partial f(X(t), t)}{\partial X(t)} \right|_{X(t)=\hat{X}(t)} \quad (4)$$

which is then used to propagate the estimator's error covariance matrix using the equation:

$$\dot{P} = AP + PA^T + Q \quad (5)$$

Process covariance matrix  $Q$  is usually chosen diagonal with the same size as state covariance  $P$ . The entries in  $Q$  are the instruments in tuning the Extended Kalman filter convergence time if measurement covariances are fixed. An initial guess can be obtained from the IMU unit. More extensive modeling of the noise certainly helps in tuning the filter. In addition the continuous time propagation equations can be replaced with discrete time. This will allow the square root implementation of the Kalman filter which results in a more numerically robust implementation due to lower condition numbers of the square root matrices.

Note that in practice the Kalman filter is actually implemented as two separate Kalman filters each having 7 states. The inner Kalman filter estimates the attitude of the helicopter and the rotational biases of the gyroscopes. The second Kalman filter estimates the position and velocities of the helicopter. The errors in the attitude are used by the second Kalman filter for correcting the position and velocity estimates but only the IMU is used for calculating the attitude estimates.

## 2.5 Update Phase

When updates of DGPS, AHRS, stereo or vision based measurements occur, an optimal discrete update is made of

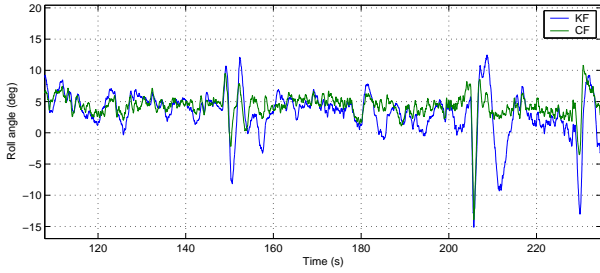


Figure 6: KF and CF comparison at estimating roll angle.

the state vector and the state vector error covariance matrix, using the equations

$$\begin{aligned}
 K &= PC^T [CPC^T + R]^{-1} \\
 \hat{X}^+ &= \hat{X} + K[\hat{z} - h(\hat{X})] \\
 P^+ &= P - KCP
 \end{aligned} \tag{6}$$

where  $h(\cdot)$  is the measurement function of the particular sensor to be updated,  $C$  is a matrix containing the partial derivatives of  $h(\cdot)$  with respect to the states. The matrix  $R$  is the measurement noise  $\hat{z}$  is the actual measurement, and  $K$  is the Kalman gain matrix. The update equations for each sensor remain the same but the measurement matrix  $C$  and the noise in measurement  $R$  vary for each sensor.

## 2.6 Kalman filter versus Complementary filter

A comparison of the performance of the Kalman filter and complementary filter for roll angle estimation is shown in Figure 6. The Kalman filter seems more responsive to larger changes in roll angle. Also note that the complementary filter data does not match well with the Kalman filter at the low values (low spikes). This is due to a positive rate bias that increases during the flight. The complementary filter does not deal with the bias and hence consistently overestimates the roll angle. Figure 7 shows the roll gyro rate bias estimated by the Kalman filter, which clearly shows the gradual increasing rate bias as the flight progresses.

## 3 Control

At the lowest level the helicopter has a set of PID loops that maintain stability by holding the craft in hover. The *heading controller* attempts to hold the desired heading by using data from the IMU (Inertial Measurement Unit) to actuate the tail rotor. The *altitude controller* uses height obtained from the Kalman filter to control the collective and the throttle. The *pitch and roll controllers* maintain

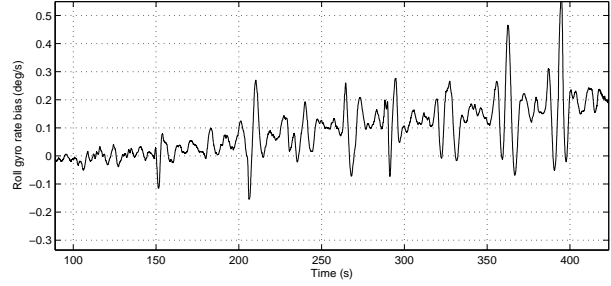


Figure 7: Roll gyro rate bias estimated by KF.

the desired roll and pitch angles received from the *lateral velocity* behavior. The *lateral velocity controller* generates desired changes in pitch and roll values that are given to the *pitch and roll controllers* to achieve a desired lateral velocity. At the top level the *navigation controller* inputs a desired heading to the *heading control*, a desired altitude or vertical velocity to the *altitude control* and a desired lateral velocity to the *lateral control* behavior.

The low-level *roll*, *pitch*, *heading* are implemented with proportional controllers (The *altitude control* behavior is implemented as a proportional-plus-integral (PI) controller). For example the *roll control* behavior reads in the current roll angle from the IMU and outputs a lateral cyclic command to the helicopter.

The *navigation controller* is responsible for overall task planning and execution. If the heading error is small, the *navigation controller* gives desired lateral velocities to the *lateral velocity*. If the heading error is large, the *heading controller* is commanded to align the helicopter with the goal while maintaining zero lateral velocity.

Both USC and the CSIRO helicopters follow the same control architecture described above. For a detailed description of the control architecture of the USC helicopter refer to [5] The difference exists in the output of the lateral velocity controller to the attitude controllers. The main difference is CSIRO velocity controller takes the current velocity and the desired velocity as inputs and outputs a desired change in angle from the initial *trim angles*. The USC velocity controller takes the current velocity and the desired velocity as inputs and outputs a desired change in angle from the *current angle* 8. The difference exists because the USC helicopter has better sensing and can estimate velocities better than the CSIRO helicopter. *During stable hover the error in velocities in the USC helicopter is 0.05 m/sec while for the CSIRO helicopter it is 0.20 m/sec*. The CSIRO helicopter can adjust the trim angles on-line using a small integral term in the lateral velocity controller, which is necessary in gusty wind conditions.

Figure 9 shows the position (from DGPS) of the CSIRO helicopter during a hover test in gusty wind. Note that this

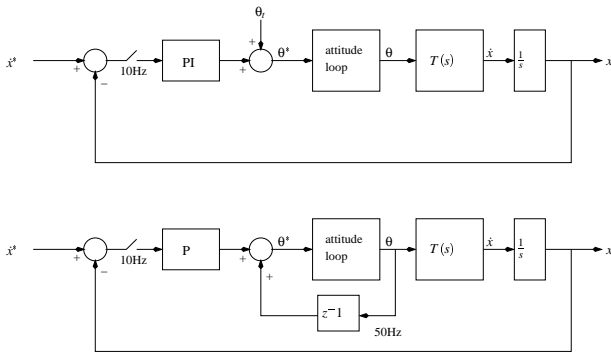


Figure 8: Different control structure of CSIRO(top) and USC(bottom) helicopters.

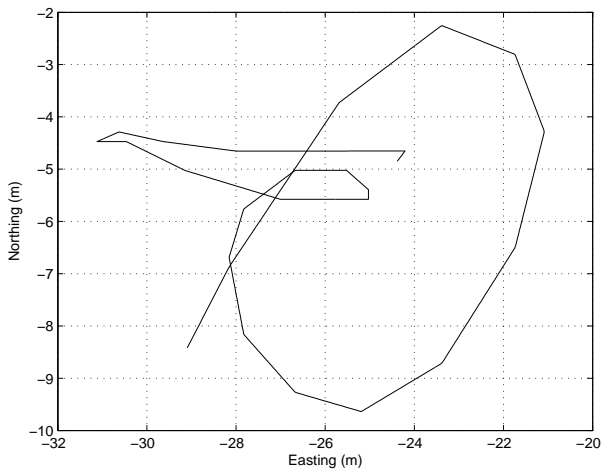


Figure 9: DGPS position during hover (velocity control only).

test did not use positions loop, only velocity loops.

## 4 Conclusion

This paper has presented work performed jointly between the USC and CSIRO helicopter teams. The work has concentrated on achieving autonomous hover of a small helicopter using low-cost sensors. Automatic control of a helicopter requires good sensing. In particular, very good velocity and attitude information is required to achieve a stable hover.

The USC helicopter uses a high-cost RT2 GPS and medium-cost IMU and magnetometers. This results in high-accuracy velocity and attitude measurements. The implications of this ‘good sensing’ for control are the ability to control the attitude in such a way that the helicopter is extremely stable in hover and naturally adjusts for wind

changes.

The CSIRO helicopter uses low-cost DGPS, vision and IMU/magnetometer. This results in relatively low-accuracy velocity and attitude measurements, which in turn leads to a control system that is capable of hover, but does not have the ability to rapidly adjust as to wind gusts.

## Acknowledgments

The authors would like to thank the rest of the CSIRO helicopter team: Graeme Winstanley, Leslie Overs, Pavan Sikka, Elliot Duff, Matthew Dunbabin, Stuart Wolfe, Stephen Brosnan, and Craig Worthington, and our pilot Fred Proos. Sri’s visit to CSIRO was part funded by USC and an ARC Discovery Grant DP0342849. The USC helicopter project is supported in part by NASA under JPL/Caltech contract 1231521, by DARPA under grant DABT63-99-1-0015 as part of the Mobile Autonomous Robot Software (MARS) program, and by ONR grant N00014-00-1-0638 under the DURIP program.

## References

- [1] A. Conway, *Autonomous control of an Unstable Model helicopter Using Carrier Phase GPS Only*. PhD thesis, Dept Electrical Engineering, Stanford University, Stanford, CA 94305, March 1995.
- [2] T. Koo, H. Shim, and O. Shakernia, “Hierarchical hybrid system design on berkely uav,” in *International Aerial Robotics Competition*, 1998.
- [3] R. Miller, O. Amidi, and M. Delouis, “Arctic test flights of the cmu autonomous helicopter,” in *Association for Unmanned Vehicle Systems International 1999. 26th Annual Symposium.*, vol. Received before publications, yet to get details., (Baltimore, MD), 1999.
- [4] G. Buskey, J. Roberts, P. Corke, P. Ridley, and G. Wyeth, “Sensing and control for a small-size helicopter,” in *Experimental Robotics* (B. Siciliano and P. Dario, eds.), vol. VIII, pp. 476–487, Springer-Verlag, 2003.
- [5] S. Saripalli, J. F. Montgomery, and G. S. Sukhatme, “Visually-guided landing of an unmanned aerial vehicle,” *IEEE Transactions on Robotics and Autonomous Systems*, 2003(to appear).
- [6] R. E. Kalman, “A new approach to linear filtering and prediction problems,” *Trans ASME*, vol. 82, pp. 35–45, March 1960.
- [7] M. Jun, S. I. Roumeliotis, and G. S. Sukhatme, “State estimation of an autonomous flying helicopter,” in *IEEE/RSJ International Conference on Intelligent Robots and Systems*, pp. 1346–1353, October 1999.